AIAA SciTech Forum
7-11 January 2019, San Diego, California
AIAA Scitech 2019 Forum

10.2514/6.2019-1897

Generalized eigenvalue approach for dynamic mode decomposition

Wei Zhang* and Mingjun Wei†
Kansas State University, Manhattan, KS, 66506, USA

As an alternative to standard Dynamic Mode Decomposition (DMD) algorithm to extract dynamics from the existed database, a generalized eigenvalue problem (GEV) was formulated and then solved by the projection to a smaller space to find the same modes. We proved their equivalence within the provided framework, while the new GEV approach showed better efficiency and accuracy. A new residue-based criterion is also developed here as a simple but rigorous way to choose dynamically important/true DMD modes from trivial/spurious modes which often appear from DMD computations.

I. Introduction

Dynamic mode decomposition (DMD) [1] is a data-driven technique to extract dynamic relevant information from time-resolved snapshots provided either by experiments or numerical simulations. Its data-driven nature makes it convenient to extract information such as dominant frequencies and spatial structures from fluid flows [2, 3] without pre-knowledge of the complex physics behind it. DMD provides a way to extract coherent structures from fluid flows [4–7], and provide base functions for the construction of reduced order models (ROM) [8–10]. Therefore, it has been gaining popularity, along with the well-known proper orthogonal decomposition (POD) and POD-based ROMs [11–21], among data analysis and model reduction techniques. DMD is also known as a numerical approximation of the spectral of Koopman operator [3, 22], a linear and infinite-dimensional operator, that can be defined in non-linear dynamic systems. The data-driven nature of DMD leads to its application of fields other than fluid flows. Grosek and Kutz [23], Erichson et al. [24] apply DMD to real-time video to subtract background for surveillance and recognition purpose. DMD is found to be effective and efficient in analyzing spatial-temporal data to study the infectious disease dynamics and plan intervention [25]. Brunton et al. [26] adapted DMD to analyze the coupled spatial-temporal neuron recording data to study the sleep spindle networks of human.

Despite the mentioned success, DMD still faces its difficulties in computation. For instance, generating the approximation matrix is time consuming and the operation to invert a matrix suffers from the singularity when data is rank deficient or nearly rank deficient. To avoid the singularity issue, a manual truncation of singular value is usually adopted by setting an artificial threshold [1]. However, the influence of truncation is not fully understood. It becomes more contradicting to one's expectation that the singularity comes from more data sampling with the intention for better accuracy. There are also concerns regarding the dynamic interpretation of some DMD modes. Efforts, such as optimized DMD [27] or sparsity promoting DMD [28], have been taken to reduce or remove spurious DMD modes.

Currently there are several numerical procedures available to identify dynamic relevant information, for example, the standard DMD algorithm by Schmid [1], the companion matrix approach adopted by Rowley et al. [3], a least square fitting approach [29] or a total least square fitting approach [30], the Koopman operator and its associated numerical methods [31]. It is noticed that all above approaches involve to compute explicitly an approximate matrix of the mapping matrix, and the computation is achieved by having a singular value decomposition (SVD) of input data followed by a matrix inversion. Even though SVD, as a common operation used by many numerical algorithms [32], is a backward stable procedure, the step of matrix inversion proposes numerical challenges when the matrix is singular or nearly singular.

In the current work, to deal with the challenge in solving the mapping matrix, we avoided solving the mapping matrix explicitly entirely. Instead, a generalized eigenvalue (GEV) problem is formulated and solved without the requirement to obtain the mapping matrix (or its approximation) directly, and solution of the GEV problem allows us to still extract dynamic information in the same way as being provided by the standard DMD method. In §II, the general framework of using GEV and its mathematical property is explained. In §III, the GEV is transformed into a more solvable form, named projected-GEV, and an efficient and stable projection is presented. Its equivalency to

*Ph.D. Candidate, Department of Mechanical and Nuclear Engineering, Student Member AIAA
†Associate Professor, Department of Mechanical and Nuclear Engineering, Associate Fellow AIAA

the standard DMD is also demonstrated. In the same session, a residue-based process is also discussed. Numerical validation is provided in §IV, and the conclusion is in §V.

II. DMD in the formulation of GEV

A. The standard DMD

The standard DMD algorithm [1] was introduced to extract dynamic relevant information form time-resolved snapshots, and is summarized below for comparison.

Let $\{\boldsymbol{x}_1, \boldsymbol{x}_2, \cdots, \boldsymbol{x}_M, \boldsymbol{x}_{M+1}\}$ be a collection of dynamic variables for a fluid dynamic system, where $\boldsymbol{x}_i = \boldsymbol{x}(t_0 + i\Delta t) \in \mathbb{R}^N$. t_0 is the initial time, $i \in \mathbb{N}$ is integer and Δt is the sampling time interval. An projection of the linear mapping onto data space is given

$$A\boldsymbol{x_i} = \boldsymbol{x}_{i+1} \tag{1}$$

Let $X = [\boldsymbol{x}_1\, \boldsymbol{x}_2\, \cdots\, \boldsymbol{x}_M]$, $Y = [\boldsymbol{x}_2\, \boldsymbol{x}_3\, \cdots\, \boldsymbol{x}_{M+1}]$, then $X, Y \in \mathbb{R}^{N\times M}$, an approximation of A is given by

$$\tilde{A} \triangleq U^T AU = U^T YV\Sigma^{-1} \tag{2}$$

where U, V, Σ is from a singular value decomposition (SVD) of $X = U\Sigma V^T$.

Inverting the matrix Σ becomes difficult when X is rank deficient or nearly rank deficient, as some smallest singular values are 0 or close to 0. The singular values truncation is advised [1] to avoid such issue. However, the influence of the truncation is not clear.

B. The GEV formulation for DMD

The algorithm proposed here to avoiding above issue is to use the generalized eigenvalue problem to capture dynamics relevant information.

Assume the same collection of data and matrix notation as in the previous section and the same linear relation given by (1). We further assume X to be a good sampling of the dynamic system, such that any interested system state $\boldsymbol{v}$ can be represented by a linear combination of X. Then the following generalized eigenvalue problem

$$Y\boldsymbol{v} = \lambda X\boldsymbol{v} \tag{3}$$

captures the dynamic information such as frequency and growth rate by λ, and dynamic modes by $X\boldsymbol{v}$. That is

$$A(X\boldsymbol{v}) = Y\boldsymbol{v} = \lambda(X\boldsymbol{v}). \tag{4}$$

It is readily verifiable that the eigenpairs of GEV (3) satisfy the standard eigenvalue problem (SEV) of (4). To make it a sufficient condition, we assumed X to be a good sampling of the dynamic system, then the interested eigenvector can be expressed by the linear combination of X. Let's say $(\lambda,\ X\boldsymbol{v})$, is the eigenpair of A. Substituted into the standard eigenvalue problem of A and make use of linear relation (1), we derived the GEV (3), thus proved the reversed statement is conditionally true.

The assumption of 'good' sampling can be further relaxed. If only the eigenvector representable by the data space is interested, the GEV formulation still computes correct eigenvectors. The relaxation may be useful in the case when X is a partial sampling of the dynamic system, but only some dominant flow structures and frequencies are desired.

The GEV formulation (3) captures the same dynamic relevant information as the standard DMD algorithm. It is a 'matrix-free' method, and the generalized eigenvalue problem circumvents the singular issue by its definition.

However, the GEV problem is more complicated than the SEV problem. To better understand the structure of eigenpairs of GEV and prepare for the numerical solution, the following section introduces the relevant theories.

C. Introduction to GEV problem

The eigenvalue of matrix pair (Y, X) is more familiar as the eigenvalue of matrix pencil $Y - \lambda X$ (a family of matrices parameterized by λ) in many matrix theory monographs. The generalized eigenvalue problem is to find the λ such that the pencil $Y - \lambda X$ is rank deficient and corresponding kernel if required.

Not like the SEV, where a full set of finite eigenvalues is guaranteed if counting the algebraic multiplicity. A fundamental difference is that GEV does not guarantee the existence of eigenvalues or eigenvectors at all. An illustrative example is given by

$$A = \begin{bmatrix} 1 \\ \alpha \end{bmatrix}, \quad B = \begin{bmatrix} 1 \\ \beta \end{bmatrix}. \tag{5}$$

If $\alpha \neq \beta$, there is no eigenvalue for pencil $A - \lambda B$. The concept of an invariant subspace is central to the SEV problem. The invariant subspace gives the solution of the eigenvalue problem. A generalization of invariant subspace to the GEV is the deflating subspace. Let (A, B) be a matrix pair, and let $(\mathcal{S}, \mathcal{U})$ be a pair of subspaces of $\mathbb{C}^n$ and of the same dimension k. Then $(\mathcal{S}, \mathcal{U})$ is called a deflating pair for (A, B) if $A\mathcal{S} \subseteq \mathcal{U}$ and $B\mathcal{S} \subseteq \mathcal{U}$. A necessary condition for (3) is the existence of non-empty deflating subspace.

One more difference is that GEV generalize eigenvalue to include infinity number. If X is singular, $\boldsymbol{c}$ is a nontrivial vector in the kernel of X and $Y\boldsymbol{c}$ is nontrivial. We call $(\infty, \boldsymbol{c})$ the eigenpair of the (3). In fact, eigenvalue λ is generalized as the ratio of two variables α, β in numerical computation [33], such that the GEV is written

$$\beta A\boldsymbol{v} = \alpha B\boldsymbol{v}. \tag{6}$$

The finite eigenvalue is given $\lambda = \alpha/\beta$ when $\beta \neq 0$. When B is singular, let vector $\boldsymbol{c}$ is in the null space of B. If $\boldsymbol{c}$ is not a null vector of A, then $\alpha \neq 0, \beta = 0$ and $\boldsymbol{c}$ are the solution of $\beta A\boldsymbol{c} = \alpha B\boldsymbol{c}$. Thus $\lambda = \alpha/\beta = \infty$ is the infinity eigenvalue. If, however, $\boldsymbol{c}$ is also the null vector of A. Arbitrary α, β satisfy (6), and all $\lambda \in \mathbb{C}$ are eigenvalues. Under this situation, λ provides no meaningful knowledge of the GEV problem as it contaminates all the meaningful eigenpairs. It is an ill-posed problem and should be avoided.

At this stage, let's introduce the essential idea regarding the structure of eigenpairs, the regular pencil or singular pencil [34] and the relevant theory.

Definition 1 *A pencil of matrices $A - \lambda B$ is called regular if*

- *A and B are square matrices of the same order n.*
- *The determinant $|A - \lambda B|$ does not vanish identically.*

In all other cases ($m \neq n$, or $m = n$ but $|A - \lambda B| \equiv 0$), the pencil is called singular.

1. The eigen structure of regular matrix pencil

As stated by the definition, a matrix pencil can only be regular if they are square matrix. And from the definition, either $|A| \neq 0$ or $|B| \neq 0$ makes a regular pencil. However, it is also possible to have $|A| = |B| = 0$, such $|A - \lambda B|$ does not vanish identically.

$$A = \begin{bmatrix} 1 & 0 \\ 0 & 0 \end{bmatrix}, \quad B = \begin{bmatrix} 0 & 0 \\ 0 & 1 \end{bmatrix}. \tag{7}$$

$|A - \lambda B| = \lambda$ vanish only at 0. We can verify 0 and ∞ are the two eigenvalues and $[0, 1]^T$, $[1, 0]^T$ are the two corresponding eigenvectors. In fact, regular pencil requires the square matrices A and B shares empty null space.

For regular pencil, there exist a full set of eigenvalues [35] if counting the infinite eigenvalues and the algebraic multiplicities. The eigenvalue is revealed by the generalized Schur decomposition of the matrix pencil.

Theorem 1 (generalized Schur theorem) *Let $A, B \in \mathbb{C}^{n\times n}$. Then there exist unitary $Q, Z \in \mathbb{C}^{n\times n}$ and upper triangular $T, S \in \mathbb{C}^{n\times}$ such that $A = QTZ^*$ and $B = QSZ^*$. In other words,*

$$A - \lambda B = Q(T - \lambda S)Z^*$$

Then eigenvalue is calculated by $\lambda_i = t_{ii}/s_{ii}, i = 1, \cdots, n$, if $s_{ii} \neq 0$. t_{ii}, s_{ii} are the diagonal elements of T and S. λ_i is infinite if $s_{ii} = 0$. Schur theorem is non-constructive, it can not be used directly to solve eigenvalues and eigenvectors. Some popular eigensolvers are using QZ algorithm [36] or Arnoldi iterative method [37].

2. The eigenstructure of singular matrix pencil

The eigenstructure of a singular matrix pencil is more complicated. The illustrative example (5) has shown that eigenvalue of the rectangular pencil does not exist. The singular pencil case deserves more attention since for DMD problem, the data X and Y usually rectangular, forms the singular pencil.

In SEV, the structure of eigenpair is revealed by reducing the matrix to the Jordan canonical form (JCF). The Kronecker canonical form (KCF) is its generalization to GEV.

Theorem 2 *Any matrix pencil $\lambda B - A$ can be reduced to*

$$S(\lambda B - A)T = diag\{L_{l_1}, \cdots, L_{l_s}, L_{r_1}^T, \cdots, L_{r_t}^T, \lambda N - I, \lambda I - J\} \tag{8}$$

i) S, T are constant invertible row and column transformations, ii) L_k is the $(k+1) \times k$ bidiagonal pencil, iii) N is nilpotent, and both N and J are in Jordan canonical form.

$$L_k = \begin{bmatrix} \lambda & & \\ -1 & \ddots & \\ & \ddots & \lambda \\ & & -1 \end{bmatrix}.$$

The Jordan block, if exist, $\lambda I - J$ reveals the finite eigenvalue of the system, while nilpotent block $\lambda N - I$ computes the infinite eigenvalues. The corresponding eigenvectors are obtained by solving the eigenvectors of the corresponding block and then do a coordinate transformation. A detailed description of Kronecker canonical form using the elementary divisors is given by Gantmakher [34, ch. XII]. An intuitive explanation with regarding the solution of the linear differential equation is given by Wilkinson [38].

Direct calculating KCF poses the same numerical difficulties as the Jordan form. A numerically stable algorithm that unitarily transforms two matrices to low triangular blocks called the pencil algorithm is given by Van Dooren [39]. The eigenvalues and eigenvectors can be computed by the corresponding blocks in the resultant decomposition.

III. DMD by projected-GEV

Though the eigenvalues can be solved by the so-called pencil algorithm, it is generally expensive. In this section, we propose a simple method that orthogonally projects the GEV problem to the data space and solves the eigenvalue problem in a Galerkin manner. The projected eigenvalue system admits spurious eigenvalues and eigenvector. Thus posterior filtering is carried out. Then a fast and numerical stable projection is proposed.

A. The Galerkin approach

The more efficient and robust method is to solve the GEV in following Galerkin manner.

$$P^T Y \boldsymbol{v} = \lambda P^T X \boldsymbol{v}, \quad X, Y, P \in \mathbb{R}^{N \times M}. \tag{9}$$

It can be seen the eigenpairs of GEV (3) is a subset of the of projected one (9), thus captured if exist. The projection transforms the GEV of size $N \times M$ to $M \times M$, reducing the size when $N > M$. The small square matrix pencil is simple both in theoretical and numerical aspect than the original big rectangular matrix. The simplest projection comes by let P to be X or Y. Since we assume X is a good sampling for the state variables, we let $P = X$. $X^T X$, $X^T Y$ only takes $2Nm^2$ multiplication operation counts.

As for the robustness, we notice if $|X| \neq 0$, $|P^T X| \neq 0$. By the continuity property of determinant, we know there exist δ and a matrix $||E|| < \delta$, $E \in \mathbb{R}^{N \times M}$, such that $|P^T(X + E)| \neq 0$. Then the eigenpairs exist and continuously change with the perturbation. Our approach is robust to small perturbation for nonsingular X.

It is easy to show that the residue of eigenpair for A equals that for GEV (3)

$$\boldsymbol{r} = A(X\boldsymbol{v}) - \lambda(X\boldsymbol{v}) = Y\boldsymbol{v} - \lambda X\boldsymbol{v}. \tag{10}$$

The residual vector is orthogonal to space $\mathcal{S}(P) = span\{\boldsymbol{p}_1, \cdots, \boldsymbol{p}_M\}$, where $\boldsymbol{p}_i$ is the column vector of P. If X is adopted as the projection matrix, the residue is orthogonal to the state space $\mathcal{S}(X)$. As we increase the sampled snapshots to include more information, the projection approach will gives increasingly accurate results.

B. filter out the spurious mode

One issue of the projection approach is that it admits spurious eigenvalues and eigenvectors since the eigenpair of projected GEV (9) is not limited to the ones of GEV (3). To filter out those spurious modes the residue is calculated.

$$||\boldsymbol{r}|| = \frac{||Y\boldsymbol{v} - \lambda X\boldsymbol{v}||}{||Y\boldsymbol{v}||} \tag{11}$$

Another interesting phenomenon occurs when data covers multiple periods, say p periods, the eigenvalues usually clustered towards some points with each cluster contains p eigenvalues. Moreover, the eigenvectors are similar to each other. Looking like they are resulted by perturbing a Jordan block of order p. Multiplicities happen especially when sampling interval aligns with a period of the dynamic system, that is, there exists an integer q, such that the sampling interval Δt and period of system T has relation $q\Delta t \approx T$. The clustering phenomenon was also observed in Chen et al. [27] where the authors try to optimize them out.

When such multiplicities occurs, a convenient criterion to assess the quality of those eigenpairs is to calculate the residue [40, ch. 2.7]. The tiniest residue among the clustered eigenpairs indicates it subjects to least perturbation, thus can be taken as a good approximation to the true eigenpair. For example, if $\boldsymbol{r} = A\boldsymbol{v} - \lambda\boldsymbol{v}$ is the residue of eigenpair $(\lambda, \boldsymbol{v})$, let $||\boldsymbol{v}|| = 1$, then the residue equation can be rewritten as

$$(A + \boldsymbol{r}\boldsymbol{v}^T)\boldsymbol{v} = \lambda\boldsymbol{v}. \tag{12}$$

$E \triangleq \boldsymbol{r}\boldsymbol{v}^T$ gives the perturbation matrix, and $||E|| = ||\boldsymbol{r}||$. A low residue indicates a low perturbation. The residue of the projected GEV

$$||\boldsymbol{r}'|| = \frac{||Y'\boldsymbol{v} - \lambda X'\boldsymbol{v}||}{||Y'\boldsymbol{v}||}, \tag{13}$$

gives the same quality estimation for generalized eigenvalue problem. Since tiny $\boldsymbol{r}'$ usually indicate tiny $\boldsymbol{r}$, besides $\boldsymbol{r}'$ removes the possible multiplicities. We use the $\boldsymbol{r}'$ as the criterion to pick the good quality eigenpairs.

On the other hand, a low condition number indicates the error is not sensitive to perturbation. So the error bound by the product of condition number κ and perturbation magnitude $||\boldsymbol{r}||$

$$\epsilon_i = \kappa_i ||\boldsymbol{r}_i||. \tag{14}$$

can be used instead when condition number is available.

C. Projection matrix selection

The projection in previous section was carried out assuming $P = X$. In this section, we consider the efficiency and stableness of this choices.

Notice X^TY and X^TX suffer overflow or underflow issues when computing numerically. A practical stable algorithm is given by decomposition of X by QR or SVD first and uses the resultant Q, or U for the projection. We note these two projections theoretically gives the same results, as they represent the same orthogonal projection onto data space. In fact, if two projection P_1, P_2 is related by $P_1 = P_2Q$, where Q is a non-singular matrix. The two projected GEV produce the same eigenvalues and eigenvectors if we substitute P_1 and P_2 in equation (9). Thus, if X is full column rank, then X, Q or U result in the equivalent projection. Though U and Q give the same projection and both are stable, they differ in efficiency. The typical operation counts for QR is of $2NM^2 - \frac{2}{3}M^3$ [41], slightly heavier than the direct projection by X, but cheaper than SVD. In the following manuscript, the projection method means $P = Q$, unless otherwise stated.

The projection method proposed here is equivalent to the standard DMD algorithm [1]. To see that, let the projection $P = U$, the projected GEV is

$$U^TY\boldsymbol{v} = \lambda\Sigma V^*\boldsymbol{v}. \tag{15}$$

A coordinate transformation $\boldsymbol{e} = \Sigma V^*\boldsymbol{v}$ makes the GEV to SEV

$$U^TYV\Sigma^{-1}\boldsymbol{e} = \lambda\boldsymbol{e}, \tag{16}$$

where $U^TYV\Sigma^{-1}$ is the approximation matrix calculated by standard DMD. As stated earlier, U and Q gives the same projection. Then we know the projected GEV letting $P = Q$ is equivalent to standard DMD.

However, the projected GEV method is more efficient than the standard DMD algorithm. The saving of an SVD decomposition can be beneficial when the data size is large. Besides, the GEV has reasonable meaning when the input snapshots are singular. A singular matrix usually indicates infinity eigenvalue. On numerical aspect, the slight perturbation will perturb the infinity eigenvalues to some large finite magnitude ones. This explains sometimes eigenvalues with large magnitude appear, while no observation of significant unstable mode in the fluid system. The residue criterion can easily remove these spurious modes. The QZ algorithm can elegantly handle such near-singular matrix [36]. While for singular matrix X', the algorithm can capture the null space and corresponding infinity

eigenvalues. For another type of eigenvalue solver, the iterative method based on Arnoldi procedure [37], a null space purification is built in to solve such situation.

As a data analysis technique, the capability of parallelization is important for analyzing large or distributed data. the projected GEV method can be easily parallelized due to the parallel QR decomposition [42, 43] and parallel GEV solver [44, 45] are the major components needed.

IV. Numerical results

A. Flow passed a fixed cylinder

The flow passing a two-dimensional fixed cylinder is chosen as a classical benchmark problem for its simple configuration and geometry. If Reynolds number (based on the incoming velocity and diameter of the cylinder) below the critical value of $Re_c = 46.6$, the flow is steady with two symmetrical vortices immediately behind the cylinder. For $Re_c \leq Re \leq 180$ perturbation grows, and the wake begins to wobble, eventually with vortices shedding alternatively from the upper and lower lateral sides of the cylinder. This process corresponds to a Hopf bifurcation [46]. Thus, flow with Re slightly above Re_c has two critical elements co-existing: an attracting limit cycle and an unstable equilibrium.

The data are obtained by numerically solving the governing equation. The incompressible Navier-Stokes equation is solved by the projection method [47]. A second-order central difference scheme is used for spatial discretization of the viscous term, and the 3rd-order Runge-Kutta/Crank-Nicolson scheme is used for time advancement, and the immersed boundary method (IBM) is implemented to handle the solid in the fluid. A non-conformal Cartesian mesh is used for the simulation. A staggered Cartesian grid is used to avoid the pressure-velocity decoupling. The numerical algorithm is the same as the one reported and tested in paper [48, 49]. The simulation was carried out with $Re = 50$. A total number of $450 \times 300 = 135,000$ grids. The grid is non-uniform with a minimum grid interval of 0.033 around the cylinder. The calculated $C_D^{Mean} = 1.43$, $C_L^{RMS} = 0.035$ and shedding frequency is $f = 0.125$ which are conformal to the ones from reference. Data are collected at $\Delta t = 1$ (dimensionless time). The time history of drag coefficient is shown in figure 1. In the following section, snapshots from $t = 680$ to $t = 1400$ are adopted for the DMD analysis.

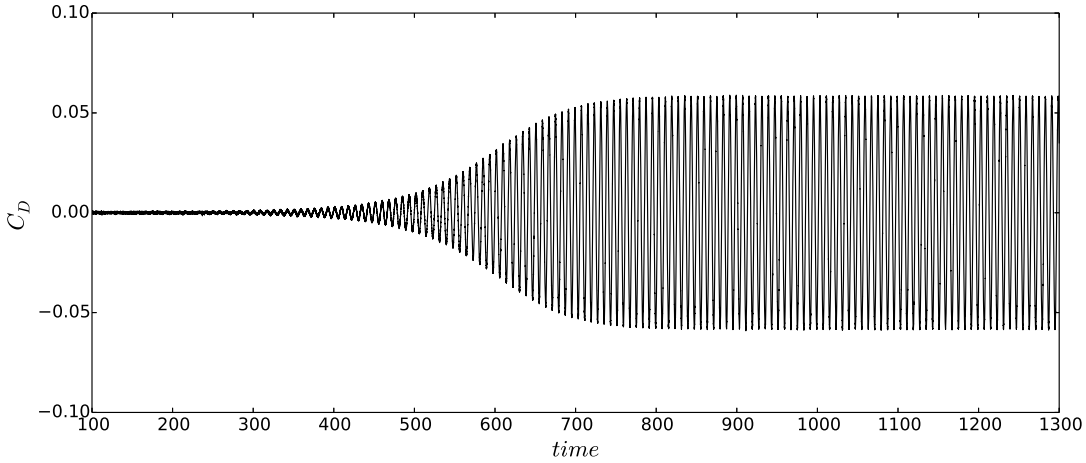

Fig. 1 The drag coefficient C_D as the function of time

B. DMD Result

Bagheri [50] studied the Koopman spectrum of this fluid system. By investigating the Perron-Frobenius operator [51], the adjoint operator of Koopman which has the same spectrum, he was able to compute the eigenvalue efficiently by forming the trace of this linear operator [52]. Since the established connection between Koopman operator with DMD algorithm [1], we can compare our results with his.

In figure 2 we present DMD eigenvalues. It is more convenient to present the dimensionless growth rate σ and

angular velocity ω instead of the eigenvalue λ by the following relation.

$$\sigma + i\omega = log(\lambda)/\Delta t \tag{17}$$

where λ is the DMD eigenvalue and Δt is the time interval between snapshots. Frequency f of DMD modes is related to the angular velocity by

$$\sigma = 2\pi f \tag{18}$$

Using the residue criterion presented in section III.B, we pick those DMD modes most accurately computed, or if the error is admissible, we can pick the modes by the energy magnitude reported by our previous report [9]. Three of the top modes near each harmonic frequency is presented.

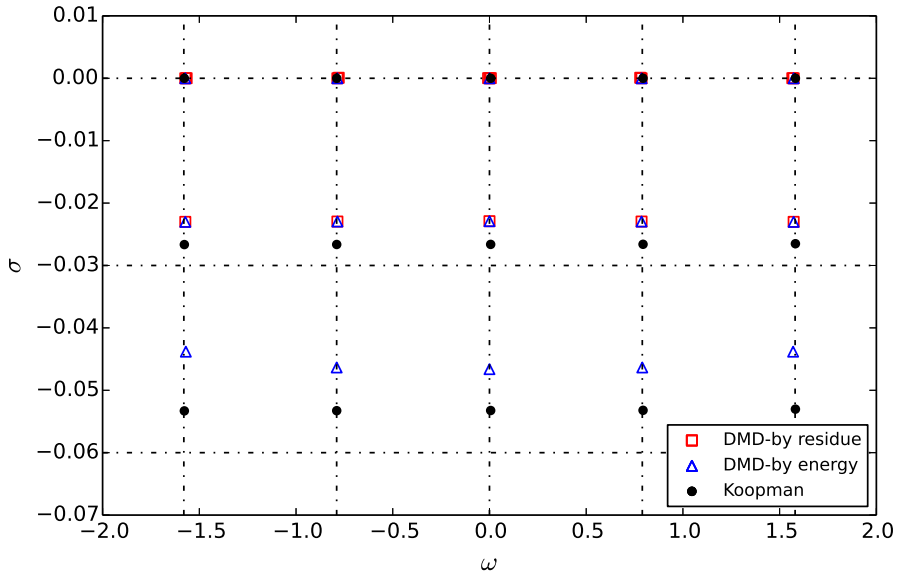

Fig. 2 The dimensionless eigenvalue ω-σ. The frequencies and growth rates are shown with (Red) square or (blue) triangle. We pick three modes near each harmonic frequency by tiny residue or most energy and label them by (red) square or (blue) triangle. (Black) solid circle represents the Koopman spectral by Bagheri [50], The dash lines are from a global stability analysis by Sipp and Lebedev [53]

In the example, we notice the lattice distribution of DMD eigenvalues discovered by Bagheri [50], following the notation of Bagheri, we denote the DMD eigenvalue by

$$\lambda_{j,m} = \sigma_{j,m} + i\omega_{j,m} \tag{19}$$

where i is imaginary number $\sqrt{-1}$, j-index represents the growth, such that $j = 0$ corresponds to the eigenvalues with $\sigma \approx 0$, $j = 1$ corresponds $\sigma = -0.023$ and so on. m-index represent the frequency, such that $m = 0$ corresponds to $\omega = 0$, $m = 1$ corresponds $\omega = \pm 0.79$ and so on. Since some of the eigenvalues coincides with others and may be not discernible in the figure, we list them in table 1. We call the modes corresponds $j = 0$ harmonic, $j = 1$ the 1st transient, and $j = 2$ the 2nd transient, except the 3nd group captured by tiny residue (hidden by the corresponding harmonic ones). Since they always evolve with a slightly different frequency with negligible growth rate, we denote them as the companion modes of the corresponding harmonic ones.

We find that the higher the order of j the eigenvalues is more sensitive to the input data. Adding or subtracting snapshots will result in the moving of (σ, ω) pairs in the complex plane. Among them, σ is more sensitive. Such phenomenon also observed by Bagheri [50].

The two criterions of residue and energy generally consider different aspects of the calculated modes. However, they usually pick some common modes. It reveals the fact that most energy modes are usually accurately captured. This is due to the fact the snapshots we used are enough to represent the possible outcome of flow status. On the other

		$m = 0$	$m = 1$	$m = 2$
harmonic	$j = 0$	(0.000, 0.000)	(0.000, 0.786)	(0.000, 1.573)
1st transient	$j = 1$	(-0.023, 0.000)	(-0.023, 0.786)	(-0.023, 1.572)
2nd transient	$j = 2$	(-0.047, 0.000)	(-0.046, 0.790)	(-0.044, 1.570)
companion	$j = 0$	(0.000, 0.007)	(0.000, 0.779)	(0.000, 1.566)

Table 1 Dimensionless eigenvalues

hand, since it focuses on the accuracy and robustness, flow pattern with low energy content can be discerned by residue criterion.

In the previous section, we mentioned the error bounds by the production of condition number and residue gives an estimation of the quality of eigenmodes. Figure 3 present the error bound, lower values means a mode accurately calculated and not sensitive to perturbation. We notice such good eigenpairs only appear near the integer multiple of shedding frequency for the 2D fix cylinder case with $Re = 50$. This frequency conforms to the fact that only 1 attracting limit cycle exists in this flow. Also, the dynamics mode captured is in corresponding to such limit cycle. With the residue or energy criterion, we can keep the true dynamic modes and remove the fake one. In figure 3 we label the top best three eigenvalues at each harmonic frequency picked either by the residue with (red) square or energy with (blue) triangle. It is obvious for every harmonic frequency, the one mode most accurately computed also plays the dominant role in the flow (energy is most significant among that particular frequency). These are the harmonic modes presented in figure 5a. The rest tiny residue mode may or may not align with the energy order.

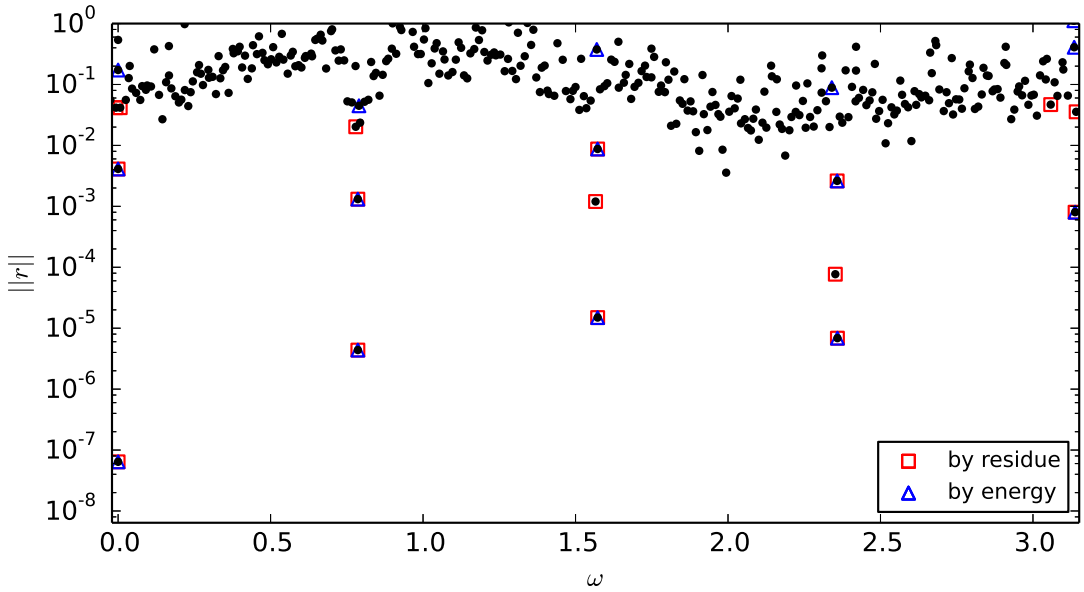

Fig. 3 The error bound for each DMD modes. (Red) square label those picked by tiny residue and (blue) triangle label those picked by bigger energy.

The energy of DMD modes is presented in figure 4, using the definition of energy in our previous report [9], with the difference of obtaining the time coefficients of these DMD modes by the least square fitting. Again we label those picked by residue or energy with the same symbols as in figure 3. From the figure, it is obvious that the most dominant modes which have the most energy are usually accurately computed by our projected GEV method. Also, the tiny residue criterion can pick modes which are less in energy but do exist in the flow. This unique character may be helpful to identify some important modes for the purpose such as controlling acoustic noise. Thanks to the high quality of our GEV formulation of DMD, such tiny modes can be revealed.

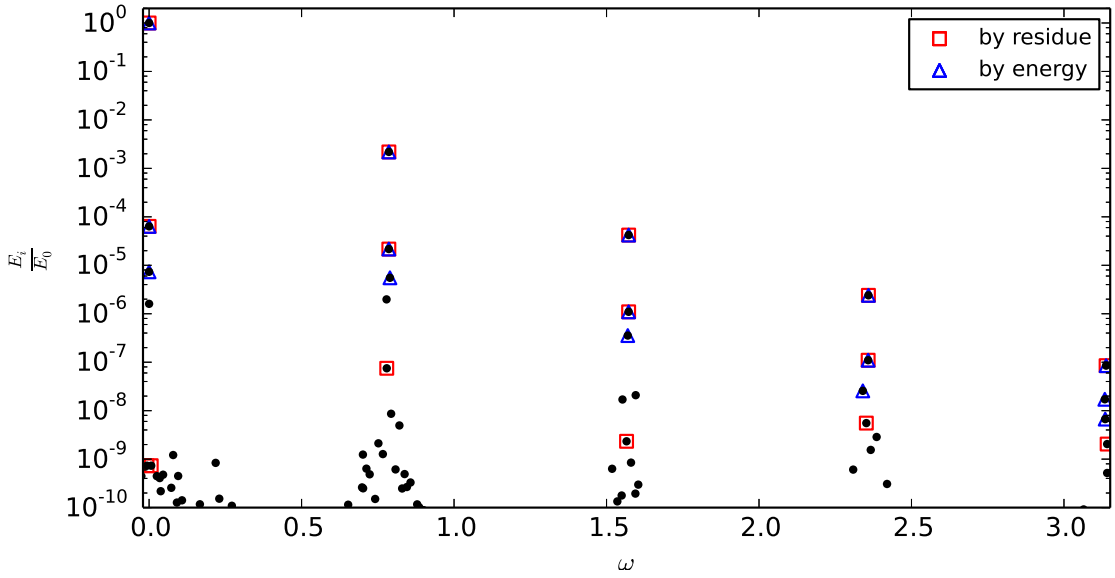

Fig. 4 The energy of each DMD modes. (Red) square label those picked by tiny residue and (blue) triangle label those picked by bigger energy.

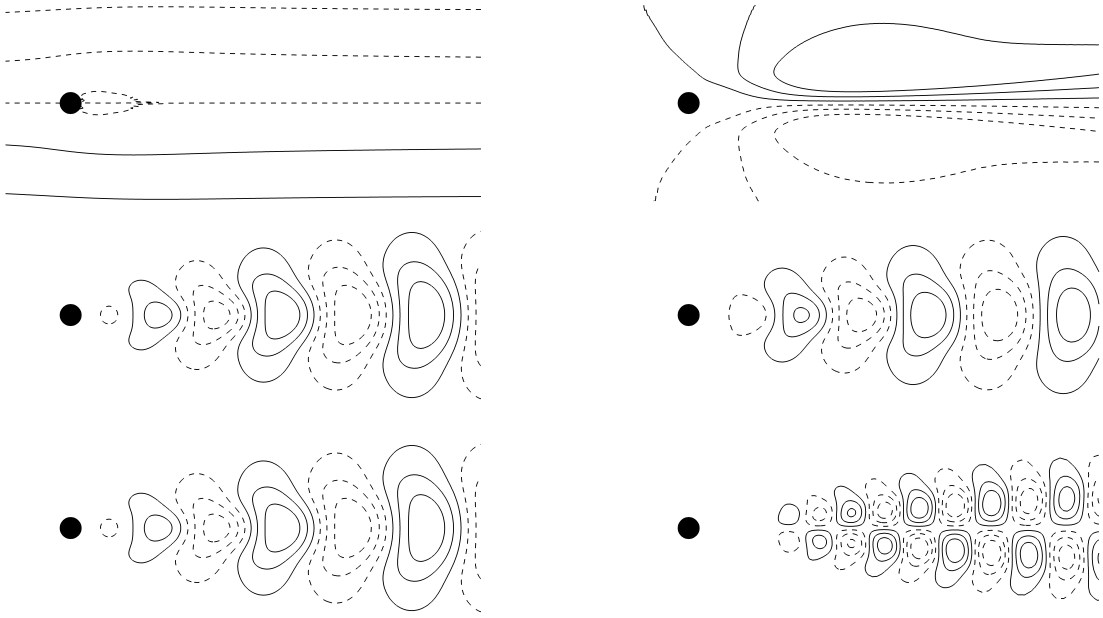

(a) Harmonic DMD modes. $\sigma = 0$

(b) 1st transient DMD modes. $\sigma \approx -0.024$

Fig. 5 Stream function of harmonic and 1st transient DMD modes. Left column is harmonic DMD modes, right column is the 1st transient DMD modes. From top to bottom $\omega = 0,\ 0.786,\ 1.573$

The harmonic modes are presented in figure 5a. The mean mode $\sigma = 0.000$, $\omega = 0.000$ captures the most energy of the flow. The first harmonic mode $\sigma = 0.000$, $\omega = 0.786$ captures the dominant vortex shedding movement in the flow. These two modes capture more than 99% energy of the whole flow. They are symmetric with respect to the centerline. The second harmonic mode $\sigma = 0.000$, $\omega = 1.573$ captures an asymmetric mode.

The first set of transient modes are shown in figure 5b. The first one is similar to the shift mode discover by [54].

It captures the transition from an unstable equilibrium to the mean flow. It is different from the mean mode or other harmonic or transient modes. The rest two modes resemble the corresponding harmonic modes but differ in some detail and magnitude.

The 2nd set of transient modes $\sigma = -0.024$ are compared with the companion modes (see table 1) in figure 6. The stream function of the 2nd set of transient modes, which are not shown here, resembles those of the first set of transient modes. We instead present their vortex structure in figure 6. The 2nd set of transient modes capture the fast decaying modes with the same structure as the 1st set of transient modes. However, they differ in magnitude and decay rate. While the companion modes (left column in figure 6) capture some modes that evolve with the same frequency as well as the same symmetries as their harmonic counterparts. However, the vortex structure differs significantly with them. They capture much smaller vortex structures.

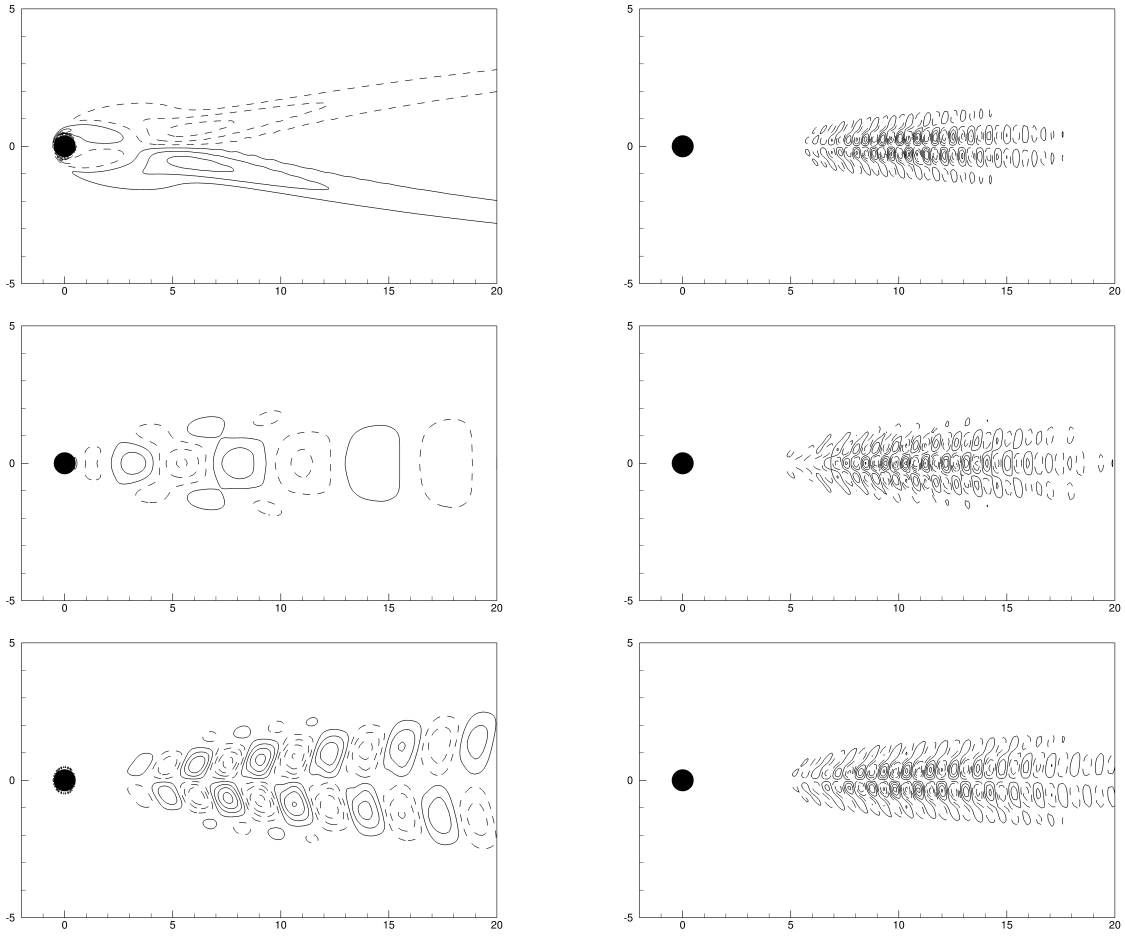

(a) 2nd transient modes. $\sigma \approx -0.047$ **(b) Companion modes.** $\sigma \approx 0$

Fig. 6 The vortex of 2nd transient modes and companion modes. Left column shows the 2nd transient modes, and right column shows the companion modes. From top to bottom $\omega \approx 0,\ 0.78,\ 1.57$

V. Conclusion

In this work, we developed a new framework to extract dynamic relevant information such as frequencies, growth/decay rates and dynamic modes by solving a generalized eigenvalue (GEV) problem. The new approach allows to calculate the mentioned dynamic information without explicitly solving the linear approximation system, thus avoiding pitfalls when the data is singular or near singular encountered in a standard DMD procedure. An efficient method is developed to solve the GEV in a projected space where the error of the approximate solution is orthogonal

to the data space, so that the residue reduces with the increase of data samples. Overall, the projected GEV approach proposed here is mathematically equivalent to the standard DMD algorithm, while the new approach shows better computational efficiency and accuracy and there is no artificial truncation involved. Due to the nature formulation of the GEV problem, it is easy to establish an error estimation for the resulted eigenpairs. Thus, it provides a convenient criterion to measure the quality of each calculated DMD eigenvalue and eigenvector.

References

[1] Schmid, P. J., "Dynamic mode decomposition of numerical and experimental data," *Journal of fluid mechanics*, Vol. 656, 2010, pp. 5–28.

[2] Schmid, P. J., "Application of the dynamic mode decomposition to experimental data," *Experiments in fluids*, Vol. 50, No. 4, 2011, pp. 1123–1130.

[3] Rowley, C. W., Mezić, I., Bagheri, S., Schlatter, P., and Henningson, D. S., "Spectral analysis of nonlinear flows," *Journal of fluid mechanics*, Vol. 641, 2009, pp. 115–127.

[4] Schmid, P. J., Meyer, K. E., and Pust, O., "Dynamic mode decomposition and proper orthogonal decomposition of flow in a lid-driven cylindrical cavity," *8th International Symposium on Particle Image Velocimetry*, 2009, pp. 25–28.

[5] Zhang, Q., Liu, Y., and Wang, S., "The identification of coherent structures using proper orthogonal decomposition and dynamic mode decomposition," *Journal of Fluids and Structures*, Vol. 49, 2014, pp. 53–72.

[6] Frederich, O., and Luchtenburg, D. M., "Modal analysis of complex turbulent flow," *TSFP DIGITAL LIBRARY ONLINE*, Begel House Inc., 2011.

[7] Seena, A., and Sung, H. J., "Dynamic mode decomposition of turbulent cavity flows for self-sustained oscillations," *International Journal of Heat and Fluid Flow*, Vol. 32, No. 6, 2011, pp. 1098–1110.

[8] Tissot, G., Cordier, L., Benard, N., and Noack, B. R., "Model reduction using dynamic mode decomposition," *Comptes Rendus Mécanique*, Vol. 342, No. 6-7, 2014, pp. 410–416.

[9] Zhang, W., and Wei, M., "Model order reduction using DMD modes and adjoint DMD modes," *8th AIAA Theoretical Fluid Mechanics Conference*, 2017, p. 3482.

[10] Bistrian, D., and Navon, I., "An improved algorithm for the shallow water equations model reduction: Dynamic Mode Decomposition vs POD," *International Journal for Numerical Methods in Fluids*, Vol. 78, No. 9, 2015, pp. 552–580.

[11] Holmes, P., Lumley, J., and Berkooz, G., *Turbulence, Coherent Structures, Dynamical Systems and Symmetry*, Cambridge University Press, New York, 1996.

[12] Wei, M., and Rowley, C., "Low-dimensional models of a temporally evolving free shear layer," *Journal of Fluid Mechanics*, Vol. 228, 2009, pp. 113–134.

[13] Wei, M., Qawasmeh, B., Barone, M., van Bloemen Waanders, B., and Zhou, L., "Low-dimensional model of spatial shear layers," *Physics of Fluids*, Vol. 24, No. 1, 2012, p. 014108.

[14] Qawasmeh, B., and Wei, M., "Low-dimensional models for compressible temporally developing shear layers," *Journal of Fluid Mechanics*, Vol. 731, 2013, pp. 364–393.

[15] Gao, H., and Wei, M., "Global model reduction for flows with moving boundary," AIAA 2014-0222. 52nd AIAA Aerospace Sciences Meeting, National Harbor, Maryland, 2014.

[16] Gao, H., and Wei, M., "Domain Decomposition in POD-Galerkin Projection for Flows with Moving Boundary," AIAA 2016-1102. 54th AIAA Aerospace Sciences Meeting, San Diego, California, 2016.

[17] Tabandeh, M., Wei, M., and Collins, J. P., "On the Symmetrization in POD-Galerkin Model for Linearized Compressible Flows," AIAA 2016-1106. 54th AIAA Aerospace Sciences Meeting, San Diego, California, 2016.

[18] Rezaian, E., and Wei, M., "Obtaining a Stable Galerkin ROM in Presence of Shock-Vortex Interactions," AIAA 2017-1008. 55th AIAA Aerospace Sciences Meeting, Grapevine, Texas, 2017.

[19] Tran, J., Gao, H., Sirohi, J., and Wei, M., "Reduced-order methodology for prediction of loads generated by a flexible flapping wing," *International Journal of Micro Air Vehicles*, Vol. 10, No. 1, 2018, pp. 31–41. doi:10.1177/1756829317708318.

[20] Rezaian, E., and Wei, M., "Eigenvalue Reassignment by Particle Swarm Optimization toward Stability and Accuracy in Nonlinear Reduced-Order Models," *2018 AIAA Fluid Dynamics Conference*, 2018, p. 3095.

[21] Gao, H., Wei, M., and Hrynuk, J., "Data-Driven ROM for the Prediction of Dynamic Stall," *2018 AIAA Fluid Dynamics Conference*, 2018, p. 3094.

[22] Mezić, I., "Spectral properties of dynamical systems, model reduction and decompositions," *Nonlinear Dynamics*, Vol. 41, No. 1-3, 2005, pp. 309–325.

[23] Grosek, J., and Kutz, J. N., "Dynamic mode decomposition for real-time background/foreground separation in video," *arXiv preprint arXiv:1404.7592*, 2014.

[24] Erichson, N. B., Brunton, S. L., and Kutz, J. N., "Compressed dynamic mode decomposition for real-time object detection," *Preprint*, 2015.

[25] Proctor, J. L., and Eckhoff, P. A., "Discovering dynamic patterns from infectious disease data using dynamic mode decomposition," *International health*, Vol. 7, No. 2, 2015, pp. 139–145.

[26] Brunton, B. W., Johnson, L. A., Ojemann, J. G., and Kutz, J. N., "Extracting spatial–temporal coherent patterns in large-scale neural recordings using dynamic mode decomposition," *Journal of neuroscience methods*, Vol. 258, 2016, pp. 1–15.

[27] Chen, K. K., Tu, J. H., and Rowley, C. W., "Variants of dynamic mode decomposition: boundary condition, Koopman, and Fourier analyses," *Journal of nonlinear science*, Vol. 22, No. 6, 2012, pp. 887–915.

[28] Jovanović, M. R., Schmid, P. J., and Nichols, J. W., "Sparsity-promoting dynamic mode decomposition," *Physics of Fluids*, Vol. 26, No. 2, 2014, p. 024103.

[29] Tu, J. H., Rowley, C. W., Luchtenburg, D. M., Brunton, S. L., and Kutz, J. N., "On dynamic mode decomposition: Theory and applications," *Journal of Computational Dynamics*, Vol. 1, No. 2, 2014, pp. 391–421.

[30] Hemati, M. S., Rowley, C. W., Deem, E. A., and Cattafesta, L. N., "De-biasing the dynamic mode decomposition for applied Koopman spectral analysis of noisy datasets," *Theoretical and Computational Fluid Dynamics*, Vol. 31, No. 4, 2017, pp. 349–368.

[31] Williams, M. O., Kevrekidis, I. G., and Rowley, C. W., "A data–driven approximation of the koopman operator: Extending dynamic mode decomposition," *Journal of Nonlinear Science*, Vol. 25, No. 6, 2015, pp. 1307–1346.

[32] Golub, G., and Kahan, W., "Calculating the singular values and pseudo-inverse of a matrix," *Journal of the Society for Industrial and Applied Mathematics, Series B: Numerical Analysis*, Vol. 2, No. 2, 1965, pp. 205–224.

[33] Kågström, B., and Poromaa, P., "Computing eigenspaces with specified eigenvalues of a regular matrix pair (A, B) and condition estimation: theory, algorithms and software," *Numerical Algorithms*, Vol. 12, No. 2, 1996, pp. 369–407.

[34] Gantmakher, F. R., *The theory of matrices*, Vol. 131, American Mathematical Soc., 1998.

[35] Wilkinson, J. H., "Kronecker's canonical form and the QZ algorithm," *Linear Algebra and its Applications*, Vol. 28, 1979, pp. 285–303.

[36] Moler, C. B., and Stewart, G. W., "An algorithm for generalized matrix eigenvalue problems," *SIAM Journal on Numerical Analysis*, Vol. 10, No. 2, 1973, pp. 241–256.

[37] Sorensen, D. C., "Implicitly restarted Arnoldi/Lanczos methods for large scale eigenvalue calculations," *Parallel Numerical Algorithms*, Springer, 1997, pp. 119–165.

[38] Wilkinson, J. H., "Linear differential equations and Kronecker's canonical form," *Recent advances in numerical analysis*, Elsevier, 1978, pp. 231–265.

[39] Van Dooren, P., "The computation of Kronecker's canonical form of a singular pencil," *Linear Algebra and its Applications*, Vol. 27, 1979, pp. 103–140.

[40] Watkins, D. S., *The matrix eigenvalue problem: GR and Krylov subspace methods*, Vol. 101, Siam, 2007.

[41] Anderson, E., Bai, Z., Bischof, C., Blackford, S., Demmel, J., Dongarra, J., Du Croz, J., Greenbaum, A., Hammarling, S., McKenney, A., and Sorensen, D., *LAPACK Users' Guide*, 3rd ed., Society for Industrial and Applied Mathematics, Philadelphia, PA, 1999.

[42] Buttari, A., Langou, J., Kurzak, J., and Dongarra, J., "Parallel tiled QR factorization for multicore architectures," *Concurrency and Computation: Practice and Experience*, Vol. 20, No. 13, 2008, pp. 1573–1590.

[43] Demmel, J., Grigori, L., Hoemmen, M., and Langou, J., "Communication-optimal parallel and sequential QR and LU factorizations," *SIAM Journal on Scientific Computing*, Vol. 34, No. 1, 2012, pp. A206–A239.

[44] Stewart, G. W., "A parallel implementation of the QR-algorithm," *Parallel Computing*, Vol. 5, No. 1-2, 1987, pp. 187–196.

[45] Maschhoff, K. J., and Sorensen, D. C., "P_ARPACK: An efficient portable large scale eigenvalue package for distributed memory parallel architectures," *International Workshop on Applied Parallel Computing*, Springer, 1996, pp. 478–486.

[46] Provansal, M., Mathis, C., and Boyer, L., "Bénard-von Kármán instability: transient and forced regimes," *Journal of Fluid Mechanics*, Vol. 182, 1987, pp. 1–22.

[47] Brown, D. L., Cortez, R., and Minion, M. L., "Accurate projection methods for the incompressible Navier–Stokes equations," *Journal of computational physics*, Vol. 168, No. 2, 2001, pp. 464–499.

[48] Yang, T., Wei, M., and Zhao, H., "Numerical study of flexible flapping wing propulsion," *AIAA journal*, Vol. 48, No. 12, 2010, pp. 2909–2915.

[49] Xu, M., Wei, M., Yang, T., and Lee, Y. S., "An embedded boundary approach for the simulation of a flexible flapping wing at different density ratio," *European Journal of Mechanics-B/Fluids*, Vol. 55, 2016, pp. 146–156.

[50] Bagheri, S., "Koopman-mode decomposition of the cylinder wake," *Journal of Fluid Mechanics*, Vol. 726, 2013, pp. 596–623.

[51] Lasota, A., and Yorke, J. A., "Exact dynamical systems and the Frobenius-Perron operator," *Transactions of the american mathematical society*, Vol. 273, No. 1, 1982, pp. 375–384.

[52] Cvitanovic, P., and Eckhardt, B., "Periodic orbit expansions for classical smooth flows," *Journal of Physics A: Mathematical and General*, Vol. 24, No. 5, 1991, p. L237.

[53] Sipp, D., and Lebedev, A., "Global stability of base and mean flows: a general approach and its applications to cylinder and open cavity flows," *Journal of Fluid Mechanics*, Vol. 593, 2007, pp. 333–358.

[54] Noack, B. R., Afanasiev, K., MORZYŃSKI, M., Tadmor, G., and Thiele, F., "A hierarchy of low-dimensional models for the transient and post-transient cylinder wake," *Journal of Fluid Mechanics*, Vol. 497, 2003, pp. 335–363.